Impact of successive freezing-thawing cycles on 3-T magnetic resonance images of the digits of isolated equine limbs

Géraldine E. Bolen, DVM, MSc; Dimitri Haye; Robert F. Dondelinger, DM, PhD; Laurent Massart, DVM; Valeria Busoni, DVM, PhD

Objective—To assess the impact of cycles of freezing and thawing on magnetic resonance (MR) images (obtained by use of a 3-T magnet) of equine feet examined ex vivo.

Sample—9 forelimbs from 9 horse cadavers.

Procedures—9 forefeet underwent MR imaging first at ambient temperature within 12 hours after the horses' death and then after each freezing-thawing cycle. Three digits underwent freezing and thawing (at 4°C for 36 hours) 2 times, 3 digits underwent freezing and thawing (at 4°C for 36 hours) once and rescanning after 24 hours at ambient temperature, and 3 digits underwent freezing and thawing at ambient temperature for 24 hours once. Images of the digits obtained prior to freezing were subjectively compared with images obtained after freezing and thawing. Changes in the signal-to-noise ratio between examinations were assessed.

Results—Overall image quality was considered unchanged except for the hoof capsule. Quantitative analysis revealed signal-to-noise ratio changes in bone marrow, soft tissues, and hoof capsule induced with both thawing processes. The signal-to-noise ratio in the synovial recess of the distal interphalangeal joint significantly increased as a result of thawing at 4°C.

Conclusions and Clinical Relevance—Although overall image quality was considered unchanged except for the hoof capsule, results suggested that changes induced in cadaver limbs following freezing and thawing, which are probably attributable both to modified and inhomogeneous temperature distribution and direct tissue damage, may alter the reliability of signal intensity in ex vivo MR examinations. (*Am J Vet Res* 2011;72:780–790)

Signs of pain are frequently localized to the feet in lame horses.[1] However, the presence of the hoof capsule makes radiographic and ultrasonographic examination of this region difficult.[1] Magnetic resonance imaging provides excellent assessment of soft tissue and osseous injuries and has become an important diagnostic tool in the evaluation of equine digits.[2–25] Because of the need for better understanding of the pathogenesis of the lesions affecting the digits of horses, comparison of MR imaging results with postmortem and histologic findings is crucial, and many research investigations are undertaken with cadaver limbs.[2,3,7,10,15,16,26–36] It is sometimes difficult to perform MR imaging of feet immediately after euthanasia or death of a horse (because of clinical case load, location of the MR unit, or other causes[37,a]) and consequently, some MR imaging procedures are conducted on frozen and thawed cadaver limbs.[7,15,16,22,26,27,34,35] A technique for optimizing preservation of equine cadaver specimens during freezing and thawing has been described.[28] However, in that study,[28]

Abbreviations

1CA	After digit was frozen then thawed at ambient temperature for 24 hours
1CR	After digit was frozen then thawed at 4°C for 36 hours
1CRA	After digit was frozen, thawed at 4°C for 36 hours, and then maintained at ambient temperature for 24 hours
2CR	After digit was frozen, thawed at 4°C for 36 hours, frozen, and thawed at 4°C for 36 hours
DDFT	Deep digital flexor tendon
DESS	Double echo steady state
DSB	Distal sesamoid bone
GE	Gradient echo
MR	Magnetic resonance
P2	Middle phalanx
P3	Distal phalanx
PD	Proton density
ROI	Region of interest
SE	Spin echo
SNR	Signal-to-noise ratio
STIR	Short tau inversion recovery
TSE	Turbo spin echo

Received November 3, 2009.
Accepted March 24, 2010.
From the Medical Imaging Section, Department of Companion Animals and Equidae (Bolen, Busoni) and Department of Animal Production (Massart), Faculty of Veterinary Medicine, and the Department of Medical Imaging, Faculty of Medicine (Haye, Dondelinger), University of Liège, 4000 Liège, Belgium.
Address correspondence to Dr. Bolen (gbolen@ulg.ac.be).

only SE images were obtained, and image changes induced by freezing and thawing were evaluated only by use of a subjective scoring method. When antemortem MR images were compared with postmortem MR images of the same feet after freezing and thawing in another study,[15] no differences were subjectively detected.

The purpose of the study of this report was to assess the impact of freezing-thawing cycles and 2 methods of thawing on SE, TSE, and GE MR images (obtained by use of a 3-T magnet) of equine feet examined ex vivo. To determine the effects of these physical conditions on the MR images, qualitative subjective image evaluation and quantitative evaluation of the SNR were used. We hypothesized that a signal change would not be detected either subjectively or quantitatively in equine cadaver digits after freezing and thawing and that the type of thawing process would not influence the signal.

Materials and Methods

Collection of the limbs—Nine fresh equine cadaver forelimbs, which were considered normal because of their appearance at inspection and findings during palpation and radiographic examination, were used for the study. Each forelimb was obtained from a different horse, all of which were routinely slaughtered at an abattoir. The limbs were sectioned at the level of the carpometacarpal joint. The proximal end of the isolated limbs was covered with an absorbent material and a latex glove to prevent blood loss during handling. The shoe was removed from each digit. The skin and the hoof were cleaned to remove foreign material, and the excess frog was trimmed. The first (baseline) MR imaging examination of each fresh limb was performed within 12 hours after death; during the interval between the death of each horse and that examination, the foot was kept at ambient temperature (approx 15° to 20°C).

Freezing-thawing procedures—After the first MR imaging examination, digits were placed in a plastic transrectal palpation glove and frozen at –25°C. Before the following MR imaging examinations, the limbs remained in the glove and the feet were either thawed in a cold room at 4°C for 36 hours or thawed at ambient temperature for 24 hours. After the first freezing-thawing cycle and subsequent MR imaging examination, the feet were placed in a new plastic glove and then frozen and thawed in the same way as for the first freezing-thawing cycle. After thawing at 4°C and before the MR imaging examination, the limbs were kept at ambient temperature for a maximum of 30 minutes.

All 9 digits underwent MR imaging within a 12-hour period after collection; these images were obtained before the limbs were exposed to any of the experimental freezing and thawing conditions (ie, baseline images of fresh limbs). The 9 digits were assigned to 3 groups (3 digits/group) and subsequently processed according to different freezing-thawing protocols. Three digits (group 1) underwent MR imaging after 1 and 2 freezing-thawing cycles as follows: images were obtained after the digits were frozen and thawed at 4°C for 36 hours (designated as 1CR images) and after the digits were again frozen and thawed at 4°C for 36 hours (designated as 2CR images). Three other digits (group 2) underwent MR imaging after 1 freezing-thawing cycle and a period at ambient temperature as follows: images were obtained after the digits were frozen and thawed at 4°C for 36 hours (1CR images) and after the thawed digits had remained at ambient temperature for 24 hours (designated as 1CRA images). The remaining 3 digits (group 3) underwent MR imaging after 1 freezing-thawing cycle, in which they were thawed at ambient temperature for 24 hours (designated as 1CA images). The duration of the first freezing period was 15 to 20 days; the duration of the second freezing period was 2 months. Thawing (via either method) was assumed to be completed on the basis of findings of a previous report[38] and confirmed by touch. The MR imaging examinations were performed within 3 months after collection of the limbs.

MR imaging examinations—Magnetic resonance images were acquired by use of a human knee radiofrequency coil in a 3-T magnetic field.[b] Images were acquired by means of an SE T1-weighted sequence in a transverse plane, TSE dual echo (T2-weighted and PD-weighted) sequence in a sagittal plane, STIR sequence in a sagittal plane, 3-D DESS sequence in a dorsal plane, 3-D GE T1-weighted fast low-angle shot sequence in a dorsal plane, and 2-D GE T2*-weighted sequence in a transverse plane (**Appendix**). The transverse plane was oriented perpendicular to the proximodistal axis of the DSB (**Figure 1**). The dorsal plane images were obtained in planes parallel to the proximodistal axis of the DSB. Image series were obtained by the same technologist together with one of the authors (GEB) by manually selecting the section prescription on the basis of a 3-plane localizer series. Anatomic features visible on the localizer images were used as reference points. Each digit

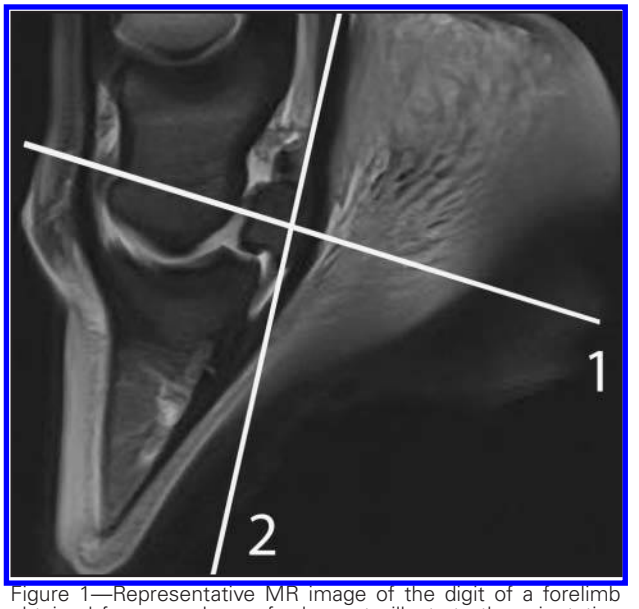

Figure 1—Representative MR image of the digit of a forelimb obtained from a cadaver of a horse to illustrate the orientation of the transverse and dorsal planes used for image acquisition in a study of the impact of successive freezing-thawing cycles on 3-T magnetic resonance images of isolated equine limbs. The lines represent the transverse plane (line 1), which was oriented perpendicular to the proximodistal axis of the DSB; dorsal plane images (line 2) were obtained in planes parallel to the proximodistal axis of the DSB.

was positioned with its dorsal aspect on the table to avoid the magic angle effect.[30]

MR image evaluation and statistical analysis—Images were evaluated in the digital imaging and communications in medicine (ie, DICOM) format on an interactive workstation.[c] The window settings used to evaluate MR images within a sequence were consistent. Co-registered images were subjectively compared side by side by a board-certified radiologist (GEB) to assess visual differences. The image evaluator was not blinded to group, and no score was used. First, visibility (contrast between structures) and margination of the anatomic structures were subjectively estimated to assess changes in image quality; for each structure (trabecular bone, synovial recesses, digital cushion, DDFT, skin and subcutaneous tissue, and hoof), image quality (visibility and margination) was defined as unchanged or deteriorated, compared with findings in baseline images of fresh digits. The signal intensity of each anatomic structure in images acquired after freezing and thawing (ie, in 1CR, 2CR, and 1CA images) were then defined by the image evaluator as isointense, hypointense, or hyperintense, compared with the signal intensity of the same structure in the baseline images. Similar assessments of signal intensity of each anatomic structure in 2CR images and 1CRA images versus findings in 1CR images were made. Sizes of the synovial recesses of the distal interphalangeal joint, the digital sheath, and the podotrochlear bursa were also subjectively estimated and defined as unchanged, reduced, or increased in size, compared with size of the respective structure in baseline images.

For each of the 9 digits, quantitative analysis to examine changes in SNR in the MR images was performed. The SNR was calculated as the ratio between the amplitude of the MR signal of the tissue (SI) and the SD of the amplitude of the background noise. Mean SI and mean SD values were calculated from 3 circular ROIs in each sequence. The ROIs were drawn by a board-certified radiologist (GEB) in the trabecular bone of each of the P3, P2, and DSB; in the palmar proximal recess of the distal interphalangeal joint; in the digital cushion; in the DDFT; in the subcutaneous tissue; and in the hoof wall. The skin and the synovial recesses of the podotrochlear bursa and of the digital sheath were not assessed quantitatively because these structures are too small to draw an ROI inside. Size of each ROI was decided subjectively in relation to the size of the anatomic structure to be evaluated. An ROI of 1 cm^2 was drawn in the distal portion of the P2, just proximal to the distal subchondral bone plate in the sagittal area. An ROI of 0.5 cm^2 was drawn in the proximal portion of the P3, just distal to the proximal subchondral bone plate in the sagittal area. For the DSB, an ROI of 0.2 cm^2 was drawn in the middle of the trabecular bone. An ROI of 0.1 cm^2 was used to assess the palmar proximal recess of the distal interphalangeal joint in the sagittal area. The digital cushion was assessed palmar to the collateral sesamoidean ligaments in the sagittal area by drawing an ROI of 2 cm^2. An ROI of 0.1 cm^2 was drawn in the DDFT proximal to the collateral sesamoidean ligament in the sagittal area. An ROI of 0.2 cm^2 was drawn in the subcutaneous tissue dorsal to the common digital extensor tendon in the sagittal area, except in dorsal images wherein measurements were obtained at the level of the DSB axial to the ungual cartilage. The hoof wall was assessed with an ROI of 0.2 cm^2 drawn in the dorsal portion of the hoof distally in the sagittal plane, except in dorsal images where the ROI was drawn in the hoof wall at the level of the DSB. An ROI of 3 cm^2 was made in the background noise in a consistent location for each sequence. The images were not coregistered for the quantitative analysis; however, the coefficient of variation was calculated for each ROI value to assess the repeatability of the value obtained by manual drawing. With the coefficients of variation, a threshold value was determined by calculating a unilateral confidence interval of 95% with a t distribution and 473 *df*.

A linear model with a mixed procedure was generated by use of computer software[d] to test the significance of SNR changes. A value of $P < 0.05$ was considered significant for all analyses.

Results

A minimal difference in section planes was sometimes evident between MR imaging examinations of the

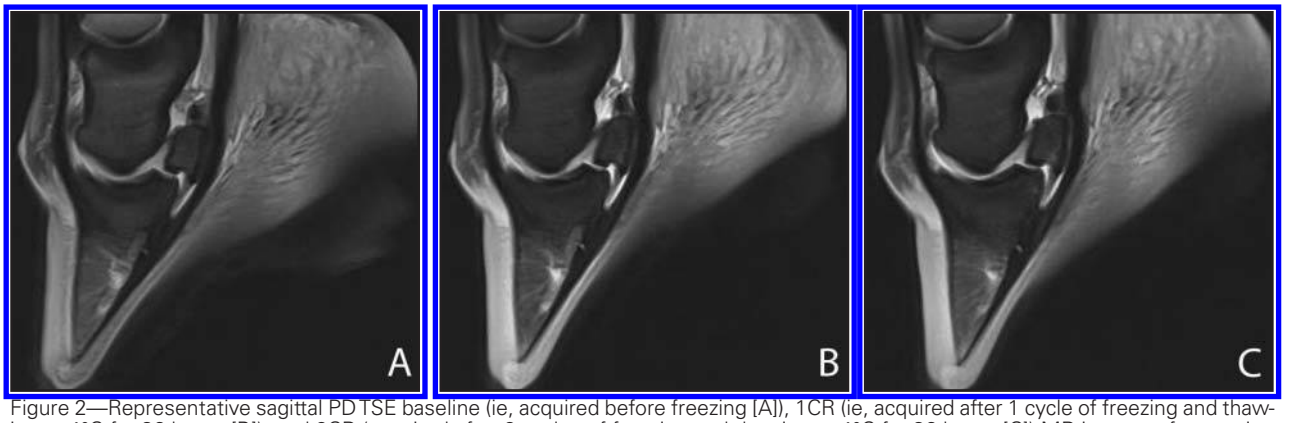

Figure 2—Representative sagittal PD TSE baseline (ie, acquired before freezing [A]), 1CR (ie, acquired after 1 cycle of freezing and thawing at 4°C for 36 hours [B]), and 2CR (acquired after 2 cycles of freezing and thawing at 4°C for 36 hours [C]) MR images of an equine cadaver digit. The duration of the first freezing period was 15 days; the duration of the second freezing period was 2 months. Subjectively, the synovial recesses, the digital cushion, and the hoof appear hyperintense in the 1CR image (B), compared with the findings in the baseline image (A). The lamina is less visible in the 1CR image (B), compared with its appearance in the baseline image (A). No changes were identified subjectively between the 1CR (B) and 2CR images (C).

Figure 3—Representative transverse T2*-weighted GE baseline (A), 1CR (B), and 2CR (C) MR images of another equine cadaver digit. For this digit, the duration of the first freezing period was 20 days; the duration of the second freezing period was 2 months. Subjectively, compared with findings in the baseline image (A), the hoof appears hyperintense, bones appear slightly hypointense, and vessels appear hyperintense in the 1CR image (B). The lamina is less visible in the 1CR image (B), compared with its appearance in the baseline image (A). No changes were identified subjectively (and confirmed statistically) between the 1CR (B) and 2CR (C) images.

same limb. Differences in section plane were mainly present at the periphery of dorsal plane images, proximally and distally. Image quality (visibility and margination) of the anatomic structures of the digits was subjectively considered unchanged except for images of the hoof in which the laminae were considered less visible (mainly distally) in the GE T2*-weighted, TSE T2-weighted, and TSE PD-weighted sequences after 1 or 2 cycles of freezing and thawing (ie, 1CR or 2CR or 1CA images), compared with the findings in baseline images of fresh limbs (**Figures 2 and 3**).

For each of the MR imaging sequences, the qualitative changes in signal intensity of the trabecular bone of the P2, P3, and DSB; synovial recesses; digital cushion; DDFT; skin and subcutaneous tissue; and hoof were determined in 1CR, 2CR, and 1CA images and compared with baseline image findings; determined in 2CR images and compared with findings in 1CR images; and determined in 1CRA images and compared with 1CR findings (**Table 1**). Signal changes were subjectively seen in most structures after freezing, compared with baseline image findings, and were more severe in soft tissues and more frequent in digits thawed at 4°C. Compared with the 1CR image findings, no subjective signal intensity changes were evident in 2CR images for any of the MR imaging sequences. For the DDFT, signal intensity did not change in 1CR, 2CR, or 1CA images, compared with baseline image findings, or in 1CRA images, compared with 1CR image findings, for any of the MR imaging sequences. The fewest differences in subjective signal intensities for the examined structures were detected between 1CRA and 1CR images. For all image sequences with the exception of the TSE T2-weighted image sequence, the proportion of examined structures that had a subjective signal intensity change from baseline was greater after freezing and thawing at 4°C for 36 hours (ie, in the 1CR and 2CR images) than it was after freezing and thawing at ambient temperature for 24 hours (ie, in the 1CA images). For 5 of the 7 MR imaging sequences, subjective signal intensity changes from baseline for the bony structures were evident in the 1CR and 2CR images but not in the 1CA images. For all 7 MR imaging sequences, the soft tissues (digital cushion, skin, and subcutaneous tissue) appeared subjectively more often hyperintense than isointense after freezing and thawing, compared with baseline image findings; the results for the soft tissue structures appeared unaffected by the freezing-thawing protocol used. The digital cushion was subjectively slightly hyperintense after 1 or 2 freezing-thawing cycles in the SE T1-weighted, TSE PD-weighted, DESS, GE T1-weighted, and GE T2*-weighted images (Figures 2, **4, and 5**); skin and subcutaneous tissue were also subjectively slightly hyperintense in those images after 1 or 2 freezing-thawing cycles, with the exception of images acquired by use of the TSE PD-weighted imaging sequence.

After freezing and thawing (regardless of the protocol used), the hoof wall appeared moderately hyperintense, compared with baseline image findings, in images obtained by means of each of the MR imaging sequences (Figures 2–4; Table 1). This signal change was more visible on the dorsal aspect and distal portion of the hoof wall in the TSE sequence (T2-weighted and PD-weighted) and in the STIR sequence images. The lamina was less visible in the GE T2*-weighted images and TSE T2- and TSE PD-weighted images after freezing and thawing, compared with baseline findings.

Subjectively, in 1CR and 2CR images, bone marrow appeared slightly hypointense, compared with baseline findings in SE T1-weighted, TSE T2-weighted, STIR, DESS, and GE T2*-weighted images (Figures 3–5). This change in bone marrow signal was more pronounced in the P2 than in the P3 or DSB and was more evident in TSE T2-weighted, STIR, and GE T2*-weighted sequence images. The bone marrow was considered hyperintense after thawing of digits at ambient temperature (ie, in 1CA images) only in TSE T2-weighted and TSE PD-weighted sequence images; no changes were seen in the images obtained via other imaging sequences. The vessels (especially those within the P3) were hyperintense in all sequence images after freezing and thawing (ie, in 1CR, 2CR, 1CRA, and 1CA images). Synovial recesses appeared mildly hyperintense (compared with baseline image findings) in 1CR and 2CR images obtained by use of the SE T1-weighted and TSE PD-weighted (Figure 2) imaging sequences and in 1CA images obtained by use of the SE T1-weighted imaging sequence. In all of the images obtained by each of the imaging sequences, no reduction in size of the synovial recesses was visible subjectively, regardless of the freezing-thawing protocol used.

The repeatability of manual drawing of ROIs was good; 93.85% (473/504) of signal values were less than the threshold in the 3 digits examined in group 1, 95.63% (482/504) of signal values were under the

Table 1—Summary of major qualitative changes identified in MR images of equine cadaver digits (n = 9) acquired by use of a 3-T magnet before and after cycles of various freezing-thawing protocols.*

Imaging sequence	Anatomic structure	Image comparison				
		1CR vs baseline	2CR vs baseline	2CR vs 1CR	1CA vs baseline	1CRA vs 1CR
SE T1	P2	↓	↓	—	—	—
	P3	↓	↓	—	—	—
	DSB	↓	↓	—	—	—
	Synovial recesses	↑	↑	—	↑	↓
	Digital cushion	↑	↑	—	↑	—
	DDFT	—	—	—	—	—
	Skin and SCT	↑	↑	—	↑	—
	Hoof	↑	↑	—	↑	—
TSE T2	P2	↓	↓	—	↑	—
	P3	↓	↓	—	↑	—
	DSB	↓	↓	—	↑	—
	Synovial recesses	—	—	—	—	↓
	Digital cushion	—	—	—	—	—
	DDFT	—	—	—	—	—
	Skin and SCT	—	—	—	—	—
	Hoof	↑	↑	—	↑	—
STIR	P2	↓	↓	—	—	↑
	P3	↓	↓	—	—	↑
	DSB	↓	↓	—	—	↑
	Synovial recesses	—	—	—	—	—
	Digital cushion	—	—	—	—	—
	DDFT	—	—	—	—	—
	Skin and SCT	—	—	—	—	—
	Hoof	↑	↑	—	↑	—
DESS	P2	↓	↓	—	—	—
	P3	↓	↓	—	—	—
	DSB	↓	↓	—	—	—
	Synovial recesses	—	—	—	—	—
	Digital cushion	↑	↑	—	↑	—
	DDFT	—	—	—	—	—
	Skin and SCT	↑	↑	—	↑	—
	Hoof	↑	↑	—	↑	—
GE T1	P2	↑	↑	—	—	—
	P3	↑	↑	—	—	—
	DSB	↑	↑	—	—	—
	Synovial recesses	—	—	—	—	—
	Digital cushion	↑	↑	—	↑	—
	DDFT	—	—	—	—	—
	Skin and SCT	↑	↑	—	↑	—
	Hoof	↑	↑	—	↑	—
GE T2*	P2	↓	↓	—	—	—
	P3	↓	↓	—	—	—
	DSB	↓	↓	—	—	—
	Synovial recesses	—	—	—	—	—
	Digital cushion	↑	↑	—	↑	—
	DDFT	—	—	—	—	—
	Skin and SCT	↑	↑	—	↑	—
	Hoof	↑	↑	—	↑	—
TSE PD	P2	↑	↑	—	↑	—
	P3	↑	↑	—	↑	—
	DSB	↑	↑	—	↑	—
	Synovial recesses	↑	↑	—	—	—
	Digital cushion	↑	↑	—	↑	—
	DDFT	—	—	—	—	—
	Skin and SCT	—	—	—	—	—
	Hoof	↑	↑	—	↑	↓

Arrows and dashes indicate the appearance of the anatomic structure in the type of image listed first, compared with findings in the type of image listed second as follows: ↓ = hypointense, ↑ = hyperintense, and — = isointense.

*All 9 digits underwent MR imaging prior to exposure to experimental freezing and thawing conditions (ie, baseline images of fresh limbs). Three digits underwent MR imaging after 1 and 2 freezing-thawing cycles as follows: images were obtained after the digits were frozen and thawed at 4°C for 36 hours (designated as 1CR images) and after the digits were again frozen and thawed at 4°C for 36 hours (designated as 2CR images). Three other digits underwent MR imaging after 1 freezing-thawing cycle and a period at ambient temperature as follows: images were obtained after the digits were frozen and thawed at 4°C for 36 hours (1CR images) and after the thawed digits had remained at ambient temperature for 24 hours (designated as 1CRA images). The remaining 3 digits underwent MR imaging after 1 freezing-thawing cycle, in which they were thawed at ambient temperature for 24 hours (designated as 1CA images). The duration of the first freezing period was 15 to 20 days; the duration of the second freezing period was 2 months; the MR imaging examinations were performed within 3 months after collection of the limbs.

SCT = Subcutaneous tissue.

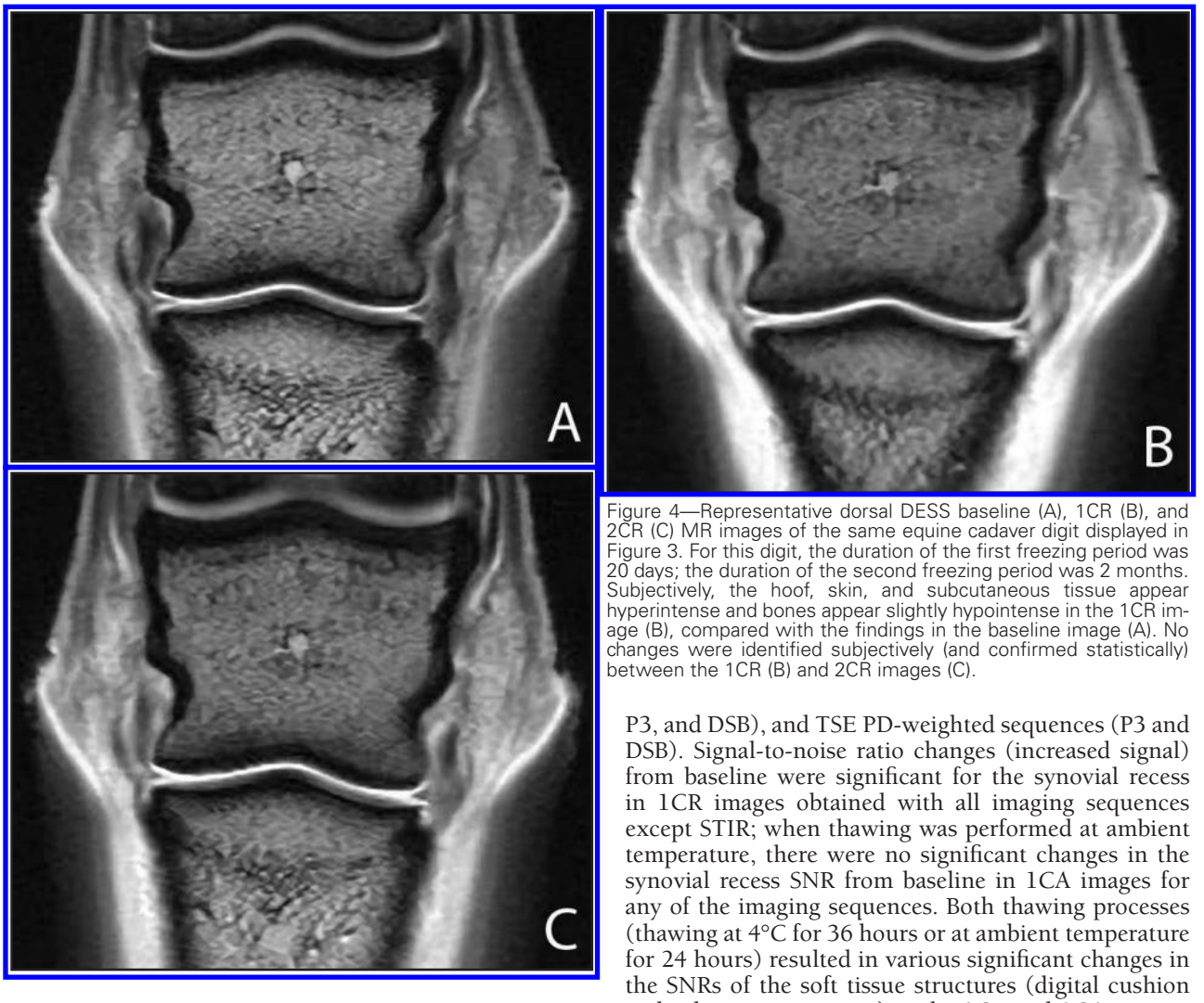

Figure 4—Representative dorsal DESS baseline (A), 1CR (B), and 2CR (C) MR images of the same equine cadaver digit displayed in Figure 3. For this digit, the duration of the first freezing period was 20 days; the duration of the second freezing period was 2 months. Subjectively, the hoof, skin, and subcutaneous tissue appear hyperintense and bones appear slightly hypointense in the 1CR image (B), compared with the findings in the baseline image (A). No changes were identified subjectively (and confirmed statistically) between the 1CR (B) and 2CR images (C).

threshold in the 3 digits examined in group 2, and 93.75% (210/224) of signal values were under the threshold in the 3 digits examined in group 3.

For each of the MR imaging sequences, quantitative analysis to examine changes in the SNR of the trabecular bone of the P2, P3, and DSB; synovial recess of the distal interphalangeal joint; digital cushion; DDFT; skin and subcutaneous tissue; and hoof were determined in 1CR, 2CR, and 1CA images and compared with baseline image findings; determined in 2CR images and compared with findings in 1CR images; and determined in 1CRA images and compared with 1CR findings (**Table 2**). The SNRs for the examined structures in 2CR images were not significantly different from the findings in 1CR images for any of the MR imaging sequences, except for the synovial recess, DDFT, and hoof in the GE T1-weighted images and subcutaneous tissue in the TSE PD-weighted images. Compared with baseline image findings, a significant SNR change for the bone marrow was detected in the P3 in the 1CA images obtained by use of an SE T1-weighted sequence. When the digits underwent 1 freezing-thawing cycle and were thawed at 4°C (ie, 1CR images), significant bone marrow SNR changes from baseline were evident in the SE T1-weighted (P2, P3, and DSB), GE T1-weighted (P2, P3, and DSB), and TSE PD-weighted sequences (P3 and DSB). Signal-to-noise ratio changes (increased signal) from baseline were significant for the synovial recess in 1CR images obtained with all imaging sequences except STIR; when thawing was performed at ambient temperature, there were no significant changes in the synovial recess SNR from baseline in 1CA images for any of the imaging sequences. Both thawing processes (thawing at 4°C for 36 hours or at ambient temperature for 24 hours) resulted in various significant changes in the SNRs of the soft tissue structures (digital cushion and subcutaneous tissue) in the 1CR and 1CA images, compared with baseline image findings; these changes were mainly seen in the GE sequence images and, with the exception of STIR images, involved an increase in SNR.

The proportion of examined structures in group 2 digits that had significant changes in SNR after 1 freezing-thawing cycle and rewarming at ambient temperature for 24 hours (ie, in 1CRA images), compared with the findings in the corresponding 1CR images, was greatest in the GE T1-weighted and TSE PD-weighted sequence images. Comparison of the 1CRA images with the 1CR images obtained by use of the 7 imaging sequences revealed that the significant changes in the SNRs of the examined structures were decreases, with the exception of the DDFT and P3 in which increases in the SNR were detected in the GE T2*-weighted sequence images and STIR sequence images, respectively.

Discussion

In the present study, the portions of cadaver limbs were removed from the MR gantry between image acquisitions, and consequently, the signal may have changed because of technical differences (eg, placement of the limb with respect to the magnet isocenter, placement of

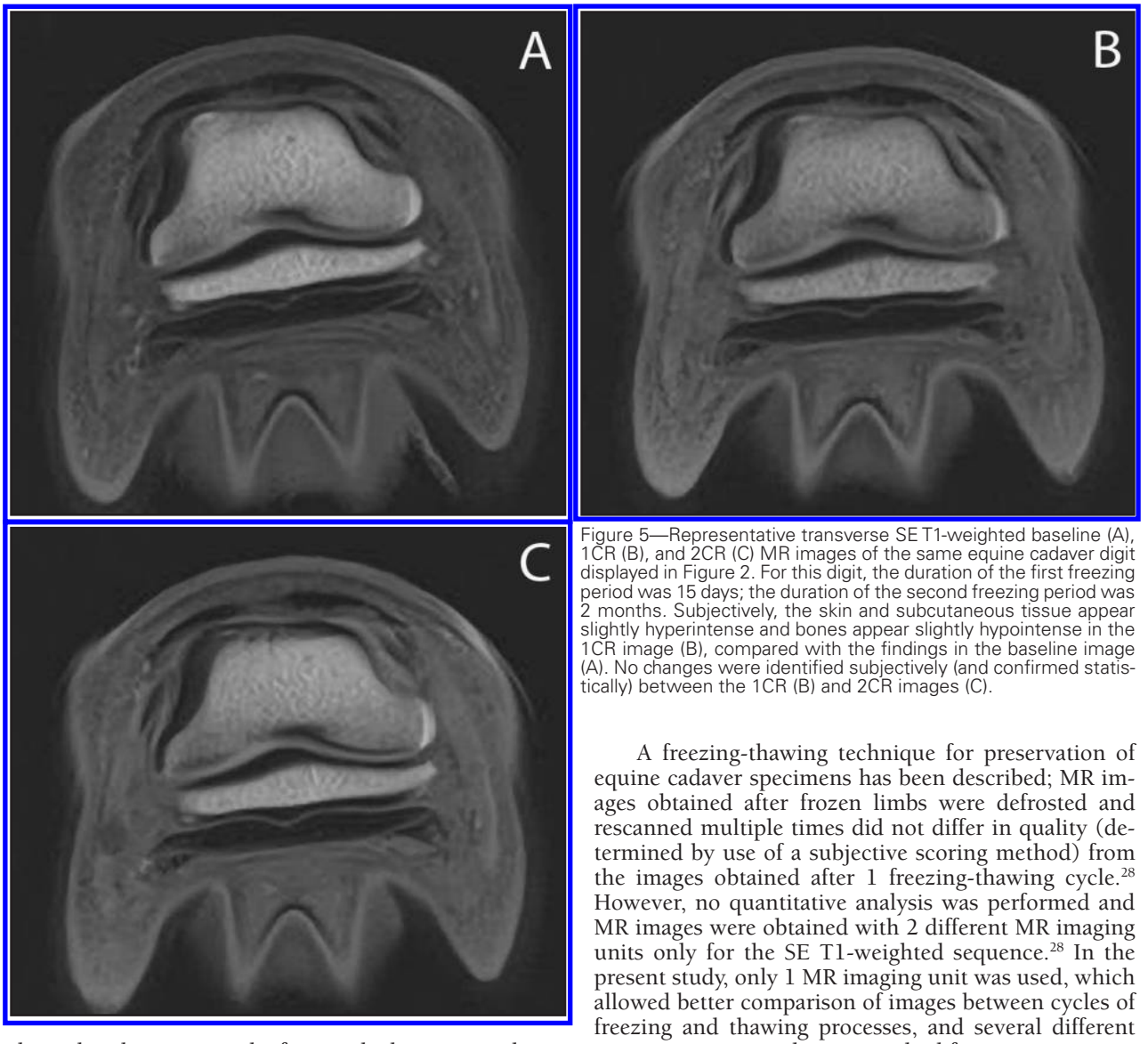

Figure 5—Representative transverse SE T1-weighted baseline (A), 1CR (B), and 2CR (C) MR images of the same equine cadaver digit displayed in Figure 2. For this digit, the duration of the first freezing period was 15 days; the duration of the second freezing period was 2 months. Subjectively, the skin and subcutaneous tissue appear slightly hyperintense and bones appear slightly hypointense in the 1CR image (B), compared with the findings in the baseline image (A). No changes were identified subjectively (and confirmed statistically) between the 1CR (B) and 2CR images (C).

the coil with respect to the foot, and adjustment values of receivers and transmitters). Thus, the SNR was calculated to evaluate signal changes instead of analyzing the absolute signal value.

Although differences in section planes among the MR imaging examinations were considered minimal, they may have potentially produced different values in the selected ROIs. However, because significant differences were seen among ROIs in trabecular bone, the synovial recess, tendons, subcutaneous tissue, and hoof and because ROIs were not drawn in peripheral areas, an influence of the section planes on the results obtained is unlikely.

The present study was not without limitations. Qualitative assessment in the present study was not done in a blinded manner and no grading system was used. Furthermore, intraobserver repeatability was not tested for this subjective analysis. The MR images were not coregistered for blinded quantitative analysis. However, the coefficient of variation was calculated for each ROI value to assess the repeatability of the value obtained by manual drawing.

A freezing-thawing technique for preservation of equine cadaver specimens has been described; MR images obtained after frozen limbs were defrosted and rescanned multiple times did not differ in quality (determined by use of a subjective scoring method) from the images obtained after 1 freezing-thawing cycle.[28] However, no quantitative analysis was performed and MR images were obtained with 2 different MR imaging units only for the SE T1-weighted sequence.[28] In the present study, only 1 MR imaging unit was used, which allowed better comparison of images between cycles of freezing and thawing processes, and several different sequences were used as in standard foot MRI examinations. In an MR microscopy study[38] of the hoof wall, there was no difference in image quality between fresh and previously frozen specimens, but signal changes were not considered. It has also been reported that there is no subjective difference between images of the same digits obtained before death and after postmortem freezing and thawing.[15] In the study of this report, antemortem MR imaging examination of the horses' limbs was not performed. However, there were differences in the procedures involved in feet preservation among the previous investigations[15,28,38] and the present study. Digits were frozen 2 hours after death of the horses and thawed at 4°C for 12 hours in the study by Keller et al,[38] whereas they were frozen within 12 hours after death of the horses and thawed at 4°C for 36 hours or at ambient temperature for 24 hours in the present study. In the study by Murray et al,[15] digits were frozen within 4 hours after death of the horses and thawed at room temperature. The interval that elapsed after death before examination of the fresh digits was performed and the conditions of thawing (rate and temperature)

Table 2—Summary of major significant quantitative changes in values of SNR in MR images of equine cadaver digits (n = 9) acquired by use of a 3-T magnet before and after cycles of various freezing-thawing protocols.*

Imaging sequence	Anatomic structure	Image comparison				
		1CR vs baseline	2CR vs baseline	2CR vs 1CR	1CA vs baseline	1CRA vs 1CR
SE T1	P2	↓	↓	—	—	—
	P3	↓	↓	—	↑	—
	DSB	↓	↓	—	—	—
	Synovial recess	↑	—	—	—	↓
	Digital cushion	↑	—	—	—	—
	DDFT	—	—	—	—	—
	SCT	↑	↑	—	—	—
	Hoof	—	—	—	—	—
TSE T2	P2	—	—	—	—	—
	P3	—	—	—	—	↓
	DSB	—	—	—	—	—
	Synovial recess	↑	↑	—	—	↓
	Digital cushion	—	—	—	—	—
	DDFT	—	—	—	—	—
	SCT	—	↓	—	—	—
	Hoof	↑	↑	—	—	↓
STIR	P2	—	—	—	—	—
	P3	—	—	—	—	↑
	DSB	—	—	—	—	—
	Synovial recess	—	—	—	—	—
	Digital cushion	—	—	—	—	—
	DDFT	—	—	—	↑	—
	SCT	↓	↓	—	—	—
	Hoof	—	—	—	—	—
DESS	P2	—	—	—	—	—
	P3	—	—	—	—	—
	DSB	—	—	—	—	—
	Synovial recess	↑	—	—	—	↓
	Digital cushion	↑	—	—	↑	—
	DDFT	—	—	—	↑	—
	SCT	↑	↑	—	↑	—
	Hoof	↑	↑	—	↑	—
GE T1	P2	↑	—	—	—	↓
	P3	↑	—	—	—	↓
	DSB	↑	—	—	—	—
	Synovial recess	↑	—	↓	—	↓
	Digital cushion	↑	—	—	↑	—
	DDFT	—	↑	↑	↑	—
	SCT	↑	↑	—	—	↓
	Hoof	↑	↑	↓	↑	↓
GE T2*	P2	—	—	—	—	—
	P3	—	—	—	—	—
	DSB	—	—	—	—	—
	Synovial recess	↑	↑	—	—	↓
	Digital cushion	—	—	—	—	—
	DDFT	—	—	—	↑	↑
	SCT	↑	↑	—	—	—
	Hoof	↑	—	—	↑	↓
TSE PD	P2	—	—	—	—	—
	P3	↑	—	—	—	↓
	DSB	↑	—	—	—	—
	Synovial recess	↑	↑	—	—	↓
	Digital cushion	↑	↑	—	—	—
	DDFT	—	—	—	—	—
	SCT	↑	—	↓	↑	↓
	Hoof	↑	—	—	—	↓

The skin and the synovial recesses of the podotrochlear bursa and of the digital sheath were not assessed quantitatively because these structures were too small to draw an ROI inside. Arrows and dashes indicate whether the SNR of the anatomic structure in the type of image listed first did or did not differ significantly from the findings in the type of image listed second as follows: ↓ = significantly decreased SNR, ↑ = significantly increased SNR, and — = no significant difference in SNR.

See Table 1 for remainder of key.

are variables that may explain differences in results among the studies. Rate of freezing may also influence the results; in a study[39] of fish, greater changes in MR parameters such as T1 and T2 values, which are in-

dicative of the signal intensity, were seen at a slower freezing rate. However, in the present study, differences in signal were detected both subjectively and quantitatively in the bone marrow and the soft tissues of the cadaver digits as a result of freezing-thawing processes. Because no quantitative analysis was performed in previous studies,[15,28,38] we speculate that mild changes in signal intensity may have been undetected.[15,28,38]

Different field strengths of the systems used (ie, a 1.5-T magnet vs a 3-T magnet) may also have allowed better detection of milder signal changes in the present study, compared with that achieved in earlier studies.[15,28,40,41] In fact, differences in image quality are related to SNR, contrast-to-noise ratio, and relative contrast[42–44] and higher SNRs and contrast-to-noise ratios are detected at higher field strengths.[40,41,45]

In the present study, image changes were subjectively and quantitatively less evident in digits that were thawed at ambient temperature for 24 hours, compared with findings in images of digits thawed at 4°C for 36 hours. This result is in accordance with data reported for cryopreservation of bovine and human spermatozoa, which indicated that less cellular damage occurs with a faster thawing process.[46,47] In the present study of equine digits, the lamina was subjectively less visible in the GE T2*-weighted, TSE T2-weighted, and TSE PD-weighted images, compared with findings in images obtained by use of the other 4 imaging sequences, and the hoof wall was hyperintense, compared with baseline findings, in MR images obtained after freezing and thawing (ie, 1CR, 2CR, and 1CA images) regardless of imaging sequence used. Because there was no subjective change in the lamina in MR images of equine cadaver feet that were refrigerated 8 to 12 hours after death,[48] early postmortem degradation is unlikely to be the cause of hoof wall changes in the present study.

Bone marrow appeared subjectively slightly hypointense in the 1CR and 2CR SE T1-weighted images, compared with baseline findings. This change was not detected after the digits in group 2 were subsequently warmed at ambient temperature, and it was not detected in the digits that were thawed at higher temperature (ie, 1CA images). Heat conduction begins at the periphery.[49] Bones are in the middle of the digit, and the P3 is located within the hoof; therefore, we may expect that the interval required for bones to thaw and reach a higher temperature is longer than that required by the surrounding soft tissues. The interval required for the P3 to thaw and warm may be even longer, considering that the horny hoof acts as thermal insulation. Magnetic resonance imaging does not yield signals for frozen materials in which all atoms have lost mobility but does yield a signal after the frozen materials thaw and reacquire molecular mobility.[28,49] In a study[50] of a frozen vertebral column specimen from a human cadaver, a complex central signal reduction artifact, which resembled an isotherm distribution, was detected via MR imaging; it was proposed that incomplete core specimen thawing had resulted in a confusing pattern of central signal dampening. In another study[51] involving an amputated human pelvic limb, reduction of the temperature of the specimen inverted the contrast between bone marrow and adipose tissue in SE T1-weighted, SE T2-weighted, and SE PD-weighted images wherein bone marrow appeared hypointense at low temperature, compared with its appearance at higher temperature. The same phenomenon may have occurred in the digits thawed at 4°C in the present study. However, because the signal reduction was not constant in all of the sequence images, other factors (eg, autolysis and water loss) may have contributed to signal changes. The hoof wall and the soft tissues appeared slightly to moderately hyperintense after freezing and thawing, compared with baseline findings. This may be attributable to a decrease of the T1 value, as detected in meat and fish after a freezing-thawing process.[52,53] The hypothesis for the decrease in T1 value is that denaturation and aggregation of proteins in frozen-thawed meat increases the effective molecular weight of the proteins[52,53] and increases magnetization transfer.[52–54] This reduces the proteins' mobility and enhances cross-relaxation (spin exchange), thereby reducing the T1 value.[52,53] In another study,[55] a significant difference in the mean T2 values of fresh and frozen-thawed trout was identified and explained by protein denaturation.

In the synovial recess of the distal interphalangeal joint of the equine cadaver digits, a significantly increased signal (compared with baseline findings) was detected in 1CR or 1CR and 2CR images obtained by use of all of the imaging sequences except STIR. In a study[56] of human synovial fluid, prolonged low-temperature (–75°C) storage resulted in a significant decrease in the signal intensities of glucose, N-acetyl glycoproteins, CH_2-chain and CH_3-terminal and resonances of lipoproteins, valine, leucine, and isoleucine obtained via MR spectroscopy. Biomolecular changes in the composition of synovial fluid may explain changes observed in the present study. However, because no significant change (compared with baseline findings) in synovial recess SNR was observed in digits thawed at ambient temperature (ie, in 1CA images) and a reverse change was seen in 1CRA images, compared with 1CR images (ie, in digits rewarmed at ambient temperature following thawing), the changes in the synovial recess SNR in the present study are more likely attributable to different specimen temperature at the time of the MR imaging examination than to the effect of the freezing-thawing process.

It is known that evaporation of moisture from the outer layers of food in frozen storage results in considerable weight losses.[53,57] A reduction in size of synovial recesses because of water loss may have been expected in the digits used in the present study, but this was not evident. In a study[57] of meat products, the least water losses were obtained by freezing boneless beef in boxes, and losses were minimal when the meat was wrapped in polyethylene bags. Preservation of intact skin and placement of the digits in a plastic glove in the present study probably helped in reducing the dehydration of tissues.

In frozen-thawed tendons used for grafts in human medicine, the fibrils appear to be enlarged and separated by wider interfibrillar gaps, compared with findings in fresh tissues that are not frozen and thawed.[58] Also, subtle edema in collagen bundles is revealed only in images that are recorded with very short echo times, whereas stronger

affections and protons in liquids between the fiber bundles were evident in images recorded with longer echo times.[59] The same phenomenon may explain signal changes seen in the DDFT after the freezing-thawing process in the present study, which were mainly seen in sequences with short echo times like GE T1-weighted, GE T2*-weighted, and DESS sequences.

Hall et al[52] reported that changes in MR images of trout and pork after 1 freezing-thawing cycle were greater than the changes that occurred between that first freezing-thawing cycle and successive freezing-thawing cycles. This is in accordance with the results of the present study, in which only minor changes were identified between the 2 successive freezing and thawing cycles (ie, in 1CR and 2CR images).

In the present study, a specific period of storage was not evaluated. Quantitative MR imaging of meat has revealed that increasing the duration of the freezing period from 2 weeks to 2 months at –18°C does not significantly enhance protein denaturation.[60] It is therefore unlikely that a relatively small difference in frozen-storage time may have contributed to changes seen in 1CR images, compared with baseline findings. However, because total storage time for digits that underwent 2 freezing-thawing cycles was longer than that for digits that underwent 1 freezing-thawing cycle, an effect of storage time cannot be excluded.

Although visibility and margination of the anatomical structures of the equine cadaver digits and overall image quality were considered unchanged (except for the hoof) in the present study, our hypothesis was rejected; the freezing-thawing processes induced changes in images of the digits, probably as a result of both modified and inhomogeneous temperature distribution and direct tissue damage. These changes may unpredictably alter the reliability of signal intensity in ex vivo MR imaging examinations; therefore, preservation conditions of cadaver specimens, including temperature and rate of thawing, should be carefully considered.

a. Van Thielen B, Murray R, De Ridder F, et al. Comparison of ultrasonography and MRI in the evaluation of palmar foot pain (abstr), in *Proceedings*. 14th Eur Soc Vet Orthop Traumatol Cong 2008;320.
b. Siemens Magnetom Trio 3T, Siemens SA, Erlagen, Germany.
c. e-Film Medical, e-Film Medical Inc, Toronto, ON, Canada.
d. SAS, version 9.1 (TS1M3), SAS Institute Inc, Cary, NC.

References

1. Dyson S. Navicular disease and other soft tissue causes of palmar foot pain. In: Ross M, Dyson S, eds. *Diagnosis and management of lameness in the horse*. St Louis: Saunders, 2003;286–299.
2. Whitton RC, Buckley C, Donovan T, et al. The diagnosis of lameness associated with distal limb pathology in a horse: a comparison of radiography, computed tomography and magnetic resonance imaging. *Vet J* 1998;155:223–229.
3. Widmer WR, Buckwalter KA, Fessler JF, et al. Use of radiography, computed tomography and magnetic resonance imaging for evaluation of navicular syndrome in the horse. *Vet Radiol Ultrasound* 2000;41:108–116.
4. Tucker RL, Sande RD. Computed tomography and magnetic resonance imaging of the equine musculoskeletal conditions. *Vet Clin North Am Equine Pract* 2001;17:145–157.
5. Dyson S, Murray R, Schramme M, et al. Magnetic resonance imaging of the equine foot: 15 horses. *Equine Vet J* 2003;35:18–26.
6. Dyson S, Murray R, Schramme M, et al. Lameness in 46 horses associated with deep digital flexor tendonitis in the digit: diagnosis confirmed with magnetic resonance imaging. *Equine Vet J* 2003;35:681–690.
7. Murray R, Dyson S, Schramme M, et al. Magnetic resonance imaging of the equine digit with chronic laminitis. *Vet Radiol Ultrasound* 2003;44:609–617.
8. Zubrod CJ, Schneider RK, Tucker RL, et al. Use of magnetic resonance imaging for identifying subchondral bone damage in horses: 11 cases (1999–2003). *J Am Vet Med Assoc* 2004;224:411–418.
9. Dyson S, Murray R, Schramme M, et al. Collateral desmitis of the distal interphalangeal joint in 18 horses (2001–2002). *Equine Vet J* 2004;36:160–166.
10. Busoni V, Heimann M, Trenteseaux J, et al. Magnetic resonance imaging findings in the equine deep digital flexor tendon and distal sesamoid bone in advanced navicular disease—an ex vivo study. *Vet Radiol Ultrasound* 2005;46:279–286.
11. Dyson S, Murray R, Schramme M. Lameness associated with foot pain: results of magnetic resonance imaging in 199 horses (January 2001–December 2003) and response to treatment. *Equine Vet J* 2005;37:113–121.
12. Kinns J, Mair TS. Use of magnetic resonance imaging to assess soft tissue damage in the foot following penetrating injury in 3 horses. *Equine Vet Educ* 2005;17:69–73.
13. Mair TS, Kinns J. Deep digital flexor tendonitis in the equine foot diagnosed by low-field magnetic resonance imaging in the standing patient: 18 cases. *Vet Radiol Ultrasound* 2005;46:458–466.
14. Zubrod CJ, Farnsworth KD, Tucker RL, et al. Injury of the collateral ligaments of the distal interphalangeal joint diagnosed by magnetic resonance. *Vet Radiol Ultrasound* 2005;46:11–16.
15. Murray R, Schramme M, Dyson S, et al. Magnetic resonance imaging characteristics of the foot in horses with palmar foot pain and control horses. *Vet Radiol Ultrasound* 2006;47:1–16.
16. Murray R, Blunden T, Schramme M, et al. How does magnetic resonance imaging represent histologic findings in the equine digit? *Vet Radiol Ultrasound* 2006;47:17–31.
17. Dyson S, Murray R. Magnetic resonance imaging evaluation of 264 horses with foot pain: the podotrochlear apparatus, deep digital flexor tendon and collateral ligaments of the distal interphalangeal joint. *Equine Vet J* 2007;39:340–343.
18. Dyson S, Murray R. Use of concurrent scintigraphic and magnetic resonance imaging evaluation to improve understanding of the pathogenesis of injury of the podotrochlear apparatus. *Equine Vet J* 2007;39:365–369.
19. Kofler J, Kneissl S, Malleczek D. MRI and CT diagnosis of acute desmopathy of the lateral collateral sesmoidean (navicular) ligament and long-term outcome in a horse. *Vet J* 2007;174:410–413.
20. Sherlock CE, Kinns J, Mair TS. Evaluation of foot pain in the standing horse by magnetic resonance imaging. *Vet Rec* 2007;161:739–744.
21. Cohen JM, Schneider RK, Zubrod CJ, et al. Desmitis of the distal digital annular ligament in seven horses: MRI diagnosis and surgical treatment. *Vet Surg* 2008;37:336–344.
22. Dyson S, Blunden T, Murray R. The collateral ligaments of the distal interphalangeal joint: magnetic resonance imaging and post-mortem observations in 25 lame and 12 control horses. *Equine Vet J* 2008;40:538–544.
23. Nagy A, Dyson S, Murray R. Radiographic, scintigraphic and magnetic resonance imaging findings in the palmar processes of the distal phalanx. *Equine Vet J* 2008;40:57–63.
24. Sherlock C, Mair T, Blunden T. Deep erosions of the palmar aspect of the navicular bone diagnosed by standing magnetic resonance imaging. *Equine Vet J* 2008;40:684–692.
25. Gutierrez-Nibeyro SD, White NA II, Werpy NM, et al. Magnetic resonance imaging findings of desmopathy of the collateral ligaments of the equine distal interphalangeal joint. *Vet Radiol Ultrasound* 2009;50:21–31.
26. Denoix J-M, Crevier N, Roger B, et al. Magnetic resonance imaging of the equine foot. *Vet Radiol Ultrasound* 1993;34:405–411.
27. Kleiter M, Kneissl S, Stanek C, et al. Evaluation of magnetic resonance imaging techniques in the equine digit. *Vet Radiol Ultrasound* 1999;40:15–22.

28. Widmer WR, Buckwalter KA, Hill MA, et al. A technique for magnetic resonance imaging of equine cadaver specimens. *Vet Radiol Ultrasound* 1999;40:10–14.
29. Asperio RM, Marzola P, Sbarbati A, et al. Comparison of results of scanning electron microscopy and magnetic resonance imaging before and after administration of a radiographic contrast agent in the tendon of the deep digital flexor muscle obtained from horse cadavers. *Am J Vet Res* 2000;61:321–325.
30. Busoni V, Snaps F. Effect of deep digital flexor tendon orientation on magnetic resonance imaging signal intensity in isolated equine limbs—the magic angle effect. *Vet Radiol Ultrasound* 2002;43:428–430.
31. Busoni V, Snaps F, Trenteseaux J, et al. Magnetic resonance imaging of the palmar aspect of the equine podotrochlear apparatus: normal appearance. *Vet Radiol Ultrasound* 2004;45:198–204.
32. Murray R, Roberts B, Schramme M, et al. Quantitative evaluation of equine deep digital flexor tendon morphology using magnetic resonance imaging. *Vet Radiol Ultrasound* 2004;45:103–111.
33. Spriet M, Mai W, McKnight A. Asymmetric signal intensity in normal collateral ligaments of the distal interphalangeal joint in horses with a low-field MRI system due to the magic angle effect. *Vet Radiol Ultrasound* 2007;48:95–100.
34. Smith M, Dyson S, Murray R. Is a magic angle effect observed in the collateral ligaments of the distal interphalangeal joint or the oblique sesamoidean ligaments during standing magnetic resonance imaging? *Vet Radiol Ultrasound* 2008;49:509–515.
35. Arble JB, Mattoon JS, Drost WT, et al. Magnetic resonance imaging of the initial active stage of equine laminitis at 4.7T. *Vet Radiol Ultrasound* 2009;50:3–12.
36. Spriet M, McKnight A. Characterization of the magic angle effect in the equine deep digital flexor tendon using a low-field magnetic resonance system. *Vet Radiol Ultrasound* 2009;50:32–36.
37. Hevesi A, Stanek Ch, Garamvolgyi R, et al. Comparison of the navicular region of newborn foals and adult horses by magnetic resonance imaging. *Physiol Pathol Clin Med* 2004;51:143–149.
38. Keller MD, Galloway GJ, Pollitt CC. Magnetic resonance microscopy of the equine hoof wall: a study of resolution and potential. *Equine Vet J* 2006;38:461–466.
39. Nott KP, Evans SD, Hall LD. Quantitative magnetic resonance imaging of fresh and frozen-thawed trout. *Magn Reson Imaging* 1999;17:445–455.
40. Niitsu M, Nakai T, Ikeda K, et al. High-resolution MR imaging of the knee at 3 T. *Acta Radiol* 2000;41:84–88.
41. Saupe N, Prussmann KP, Luechinger R, et al. MR imaging of the wrist: comparison between 1.5- and 3-T MR imaging—preliminary experience. *Radiology* 2005;234:256–264.
42. Hart H Jr, Bottomley P, Edelstein W, et al. Nuclear magnetic resonance imaging: contrast-to-noise ratio as a function of strength of magnetic field. ***AJR*** 1983;141:1195–1201.
43. Rutt B, Lee D. The impact of field strength on image quality in MRI. *J Magn Reson Imaging* 1996;6:57–62.
44. Vetter D, Kastler B. Facteurs de qualité de l'image en IRM. In: Kastler B, Vetter D, Patay Z, et al, eds. *Comprendre l'IRM, manuel d'auto-apprentissage*. 5th ed. Paris: Masson, 2003;115–131.
45. Maubon AJ, Ferru JM, Berger V, et al. Effect of field strength on MR images: comparison of the same subject at 0.5, 1.0, and 1.5 T. *Radiographics* 1999;19:1057–1067.
46. Chandler JE, Ruiz CF, Adkinson RW, et al. Relationship between final temperature, thaw rate, and quality of bovine semen. *J Dairy Sci* 1984;67:1806–1812.
47. Calamera JC, Buffone MG, Doncel GF, et al. Effect of thawing temperature on the motility recovery of cryopreserved human spermatozoa. *Fertil Steril* 2010;93:789–794.
48. Bolen G, Haye D, Dondelinger R, et al. Magnetic resonance signal changes during time in equine limbs refrigerated at 4°C. *Vet Radiol Ultrasound* 2010;51:19–24.
49. Koizumi M, Naito S, Ishida N, et al. A dedicated MRI for food science and agriculture. *Food Sci Technol Res* 2008;14:74–82.
50. Kurmis A, Slavotinek J, Barber C, et al. An unusual MR signal reduction artefact in an incompletely thawed cadaver spine specimen. *Radiography* 2009;15:86–90.
51. Petrén-Mallmin M, Ericsson A, Rauschning W, et al. The effect of temperature on MR relaxation times and signal intensities for human tissues. *Magn Reson Mater Phys Biol Med* 1993;1:176–184.
52. Hall LD, Evans SD, Nott KP. Measurement of textural changes of food by MRI relaxometry. *Magn Reson Imaging* 1998;16:485–492.
53. Evans SD, Nott KP, Kshirsagar AA, et al. The effect of freezing and thawing on the magnetic resonance imaging parameters of water in beef, lamb and pork meat. *Int J Food Sci Technol* 1998;33:317–328.
54. Virta A, Komu M, Kormano M, et al. Magnetization transfer in protein solutions at 0.1 T: dependence on concentration, molecular weight, and structure. *Acad Radiol* 1995;2:792–798.
55. Renou JP, Foucat L, Bonny JM. Magnetic resonance imaging studies of water interactions in meat. *Food Chem* 2003;82:35–39.
56. Damyanovich AZ, Staples JR, Marshall KW. The effects of freeze/thawing on human synovial fluid observed by 500 MHz 1H magnetic resonance spectroscopy. *J Rheumatol* 2000;27:746–752.
57. Bustabad OM. Weight loss during freezing and the storage of frozen meat. *J Food Eng* 1999;41:1–11.
58. Giannini S, Buda R, Di Caprio F, et al. Effects of freezing on the biomechanical and structural properties of human posterior tibial tendons. *Int Orthop* 2008;32:145–151.
59. Schick F, Dammann F, Lutz O, et al. Adapted techniques for clinical MR imaging of tendons. *Magn Reson Mater Phys Biol Med* 1995;3:103–107.
60. Guiheneuf TM, Parker AD, Tessier JJ, et al. Authentication of the effect of freezing/thawing of pork by quantitative magnetic resonance imaging. *Magn Reson Chem* 1997;35:S112–S118.

Appendix

Magnetic resonance imaging protocols used in a study to assess the impact of successive freezing-thawing cycles on 3-T MR images of the digits of isolated equine limbs.

Imaging sequence	Plane	TR (ms)	TE (ms)	FOV (cm)	Matrix	Th (mm)	Gap (mm)	Flip (°)	TA (mm)	NEX	TI
SE T1	Transverse	450	11	150–190	384 × 213	3	1.0	90	1:27	1	NA
TSE T2	Sagittal	2,790	88	168–170	384 × 266	5	0.0	180	2:10	1	NA
TSE PD	Sagittal	2,790	25	168–170	384 × 266	5	0.0	180	2:10	1	NA
STIR	Sagittal	3,080	50	153–170	320 × 230	5	0.0	180	2:17	2	180
DESS	Dorsal	12.66	4.47	156–200	448 × 245	1.5	0.3	20	1:50	2	NA
GE T1-weighted	Dorsal	8.32	4	170–170	384 × 307	1	0.2	15	1:52	1	NA
GE T2*-weighted	Transverse	450	6	170–170	320 × 256	3	1.0	20	1:41	1	NA

FOV = Field of view. NA = Not applicable. NEX = Number of acquisitions. TA = Acquisition time. TE = Echo time. Th = Thickness. TI = Inversion time. TR = Repetition time.